energies

MDPI

Article

Development of the EM Field in a Shielding Enclosure with Aperture after Interference Caused by a Subnanosecond High-Power Parallelly Polarized EM Plane Wave Pulse

Magdalena Budnarowska *, Jerzy Mizeraczyk and Kamil Bargieł

Department of Marine Electronics, Gdynia Maritime University, Morska 83, 81-225 Gdynia, Poland
* Correspondence: m.budnarowska@we.umg.edu.pl

Abstract: Due to the increase in the threat of attacks with high-power electromagnetic (EM) pulses, there is great interest in metallic enclosures with high shielding effectiveness (SE). Necessary technological apertures in these enclosures reduce their effectiveness. Understanding the penetration and internal propagation of the high-power EM pulses into an apertured enclosure is fundamental to assessing the EM SE of the enclosure. In the present paper, results of the numerical simulations of development of the EM field in a shielding enclosure with aperture after the interference of a subnanosecond high-power EM plane wave pulse of the parallel polarization (having the duration of 0.3558 ns and the amplitudes of the electric and magnetic fields of 10^6 V/m and 2.6 $\times 10^3$ A/m, respectively) are presented. The results obtained include 3D and 2D images , vector maps of the EM field developed inside the enclosure, and time-varying distributions of the electric charges formed on the inner walls of the enclosure. They revealed the mechanism of formation of the EM field inside the enclosure caused by the subnanosecond high-power parallelly polarized EM pulse. The EM field formed in the enclosure with aperture has the form of the electric and magnetic field interference structures. They are a superposition of the incident EM pulse field, which entered the enclosure through the aperture in the way described by the geometrical (ray) optics, the electric field generated by the electric charges formed on the aperture edges and inner sides of the walls of the enclosure, and the magnetic field generated by the surface current formed on the aperture edges and on the inner walls of the enclosure. The amplitudes of the electric and magnetic fields of the strongest EM interference structures decrease non-monotonically to about 0.7 $\times$ 10^5 V/m and 200 A/m at t = 5 ns. We found that the points in the enclosure are subjected to the disturbance of a long series of subnanosecond EM pulses, which we have called internal EM pulses. The amplitudes of these internal pulses are lower than those of the incident EM pulse. Nevertheless, they can pose a severe EM hazard inside the enclosure due to their large number (about 900 internal pulses in 30 ns). This means a fundamental change in the character of the EM disturbance caused by the subnanosecond pulse when the enclosure with aperture is used as a shield.

Keywords: electromagnetic interference; EMI; parallel polarization of high-power EM pulse; shielding enclosure with aperture; shielding box; electromagnetic field shielding; numerical simulation of EM field; CST Studio

Citation: Budnarowska, M.; Mizeraczyk, J.; Bargieł, K. Development of the EM Field in a Shielding Enclosure with Aperture after Interference Caused by a Subnanosecond High-Power Parallelly Polarized EM Plane Wave Pulse. *Energies* **2023**, *16*, 585. https://doi.org/10.3390/en16020585

Academic Editor: Andrea Mariscotti

Received: 21 November 2022
Revised: 20 December 2022
Accepted: 23 December 2022
Published: 4 January 2023

1. Introduction

An exponentially increasing number of electronic devices, and continuous advances in information technology, make it necessary to protect advanced electronic systems from various electromagnetic (EM) environmental threats. One of the most serious threats designed to disrupt and destroy an electronic infrastructure is an Intentional Electromagnetic Environment (IEME). These intentional disturbances are characterized by high-power EM radiation [1–4] and categorized as high-power EM environments. The radiation of high-power environments is called high-power electromagnetic (HPEM) radiation. HPEM

radiation is mostly generated in the form of pulses [5,6]. There exists a reasonable opinion that short-duration pulses with a high-power density (i.e., high electric field strength [6]) yield the most chaos in the operation of electronic apparatus. Operational disruption and, ultimately, damage to electronic components and systems are caused by the large potentials induced by HPEM pulses with their high and rapidly changing electric field strength. Overvoltage waves, electrostatic discharge, and breakdowns in semiconductor junctions are all features of the disturbance. Consequently, it is not the energy of an EM pulse that is most important but the maximum value of its electric field strength when assessing the level of EM vulnerability in electronic objects. High electric field strengths of the order 10^5-10^6 V/m [7] characterize the high-power short-duration pulses that pose the greatest threat to the operation of electronic objects.

Maintaining the proper functioning of electronic equipment and systems depends on the correct analysis of the EM field caused by an HPEM pulse followed by the development of countermeasures to eliminate or minimize the effects of the pulse. The most effective method of protecting electronic equipment and systems is so-called EM shielding. Different types of metal enclosures provide highly effective protection for electronic objects against high-power EM pulses. These may come in the form of shielding enclosures or boxes in which susceptible electronic objects can be placed. A highly conductive metal is used in the construction of these enclosures to absorb the EM energy of high-power EM pulses and generate an electric current on the surface of the enclosure body [1,6,8–10]. Sensitive electronics in the enclosure are protected as the current is absorbed through a ground connection or virtual ground plane. This concept also operates in the opposite direction, i.e., any EM signals formed within the enclosure are protected from being transmitted uncontrolled outside the box (any signal transmission takes place in a controlled manner through shielded wire connections). Police, military and intelligence agencies, banking systems, government organizations, etc., use large EM shielding enclosures to protect critical electronic systems. More recently, those involved in consumer and industrial electronics, and emergency services, have shown a growing interest in EM shielding for small devices such as smartphones, ID cards, laptops, tablets, and car keys [2,4,11]. Ideal protection for all but low-frequency magnetic fields is provided by a fully enclosed, perfectly conductive EM shielding box. Unfortunately, fully enclosed boxes are not practical. Various apertures in them are usually required for purposes such as ventilation or wire connections for communication purposes. These functional requirements mean EM protection can never be perfect. The interference caused by external EM sources depends on their coupling into the enclosure and the sensitivity of protected objects to the spatial, temporal, and frequency properties of the external EM interference. For this reason, determining the effects of HPEM pulse penetration into the enclosure through necessary technological openings plays an essential role in the design of shielding enclosures [8–10].

Determining the effects of the most probable intentional high-power EM disturbances, which are subnanosecond pulses, is crucial to understanding the interaction and coupling mechanisms of apertured shielding enclosures. Studying the temporal and spatial progression of the EM field and the coupling mechanisms occurring inside enclosures provides the opportunity to properly evaluate their shielding effectiveness and improve the design.

In this paper, we study the interaction of an ultrashort interference caused by the subnanosecond EM plane wave pulse of a Gaussian distribution of the electric and magnetic fields and parallel polarization, with a small rectangular enclosure (455 × 50 × 463 mm) having a rectangular aperture. This work continues the numerical research undertaken in the previous article [4]. Our present numerical study of the coupling and development mechanisms of the EM field concerns the case of the normally incident EM plane wave pulse, the electric field strength $\vec{E}$ vector of which was parallel to the wider walls of the enclosure (i.e., also parallel to the longer side of the rectangular aperture). The difference from the previous work is that in the previous work the normally incident EM plane wave pulse was polarized perpendicular to the wider walls of the enclosure (i.e., also perpendicular to the longer side of the rectangular aperture). The aim of the present study was to visualize

the temporal and spatial development of the electromagnetic (EM) field in the shielding enclosure with aperture after a transient interference caused by the subnanosecond high-power EM plane wave pulse with parallel polarization. The study's results were expected to be essential for a better understanding of EM field build-up in apertured enclosures. In turn, this will support the evaluation of shielding effectiveness under the conditions of ultrashort transient interference. Below we present the results that show the temporal and spatial development of the parallel polarized EM field penetrating the shielding enclosure. The results are in many aspects different than those of the perpendicularly polarized EM field presented in [4]. These differences will be the subject of another paper.

2. Shielding Enclosure with Aperture

The geometry of the shielding enclosure with aperture (hereinafter called the enclosure for brevity) is shown in Figure 1. The enclosure was placed in a rectangular coordinate system in such a way that its center was in the center of the coordinate system (point (0,0,0)). The external dimensions of the enclosure are as follows: width: 455 mm × height: 50 mm × depth: 463 mm. A rectangular aperture, 30 mm × 80 mm, was placed in the center front wall of the enclosure. Its purpose was to simulate ventilation opening and wire connection entries, typical of real-world shielding enclosures. The walls of the enclosure are 1 mm thick and made from a material with infinite conductivity, a so-called perfect electric conductor (PEC).

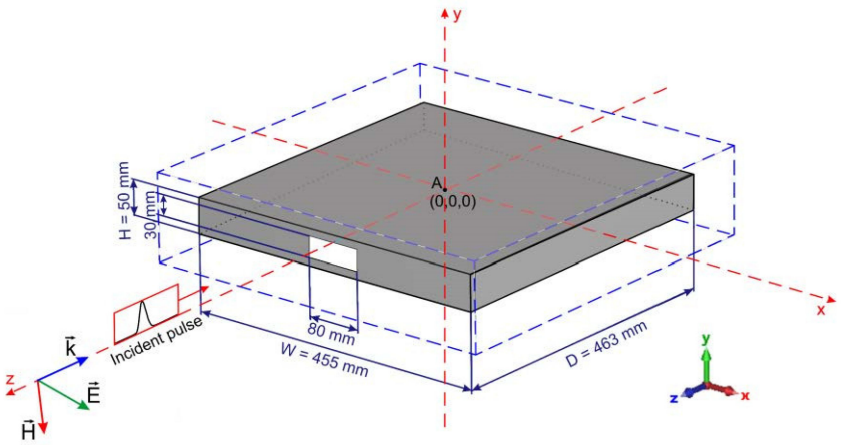

Figure 1. The geometry of the enclosure with aperture in the rectangular coordinate system. The computation area is marked in blue dashed lines. The electric field strength vector $\vec{E}$ is directed in the +x direction. The magnetic strength vector $\vec{H}$ is directed in the -y direction. Vector $\vec{k}$ shows the propagation direction of the EM incident pulse. Point A is the center of the enclosure.

3. Simulation Procedure

The numerical simulation was performed using CST Studio 2020 software equipped with the MW, RF, and Optical module for modeling and comprehensive simulations of high-frequency EM fields of 3D objects [11].

A time domain solver was used to perform numerical computations. The simulation model used a hexahedral mesh type discretized with variable-size rectangular cuboids (the cuboids define a small volume in space to calculate the electric and magnetic fields). To satisfy the requirements of calculation speed, correctness, and memory, we optimized the mesh by using 15 cells per wavelength (both near and far from the object) and divided the maximum cell size by 15 to define a minimum cell size. A singularity model was used for the PEC. The final mesh has 57, 102, and 540 mesh cells.

The dimensions of the computational area were x (−235 mm, + 235 mm), y (−32.5 mm, +32.5 mm), and z (−239 mm, +239 mm). The enclosure was placed symmetrically in the computational area marked in blue dashed lines (470 × 65 × 478 mm). The configuration

of the computational area is illustrated in Figure 1. The computation area's front plane is placed at z = +239 mm. The subnanosecond incident plane wave pulse propagates perpendicularly in the -z direction towards the front wall of the enclosure. It is assumed that the electric field strength vector $\vec{E}$ of the incident pulse is directed in the +x direction (correspondingly, the magnetic field strength vector $\vec{H}$ is directed in the $-$y direction).

4. Parameters of the Incident EM Plane Wave Pulse

It is generally recognized that the greatest threat in the operation of electronic objects is short-term pulses of high-power density, i.e., high electric field strength [2,3]. Following the above, in the numerical simulation HPEM pulse with a Gaussian distribution and subnanosecond duration was used as electromagnetic interference.

The following equation describes the time dependence of the electric and magnetic field strengths the incident pulse:

$$\frac{A(t)}{A_{max}} = e^{-\frac{4\ln 2(t-t_{max})^2}{\tau^2}}, \quad (1)$$

where

A(t)—the amplitude of the electric or magnetic field strength;
A_{max}—the maximum amplitude of the electric field or magnetic field strength;
t_{max}—the time when the amplitude of the electric or magnetic field strength reaches its maximum value;
τ—the full width at half maximum of the incident pulse.

The incident pulse parameters are shown in Figure 2: the maximum electric field strength amplitude—10^6 V/m, the maximum magnetic field strength amplitude—2.68 × 10^3 A/m, the maximum pulse power density—2.68 GW/m^2, time when the amplitude of the electric or magnetic field strengths reach their maximum values—t_{max} = 0.1779 ns, the full width at half maximum (FWHM) of the incident pulse—τ = 0.0804 ns, the pulse rise time—τ_r = 0.058 ns, the pulse fall time—τ_f = 0.058 ns.

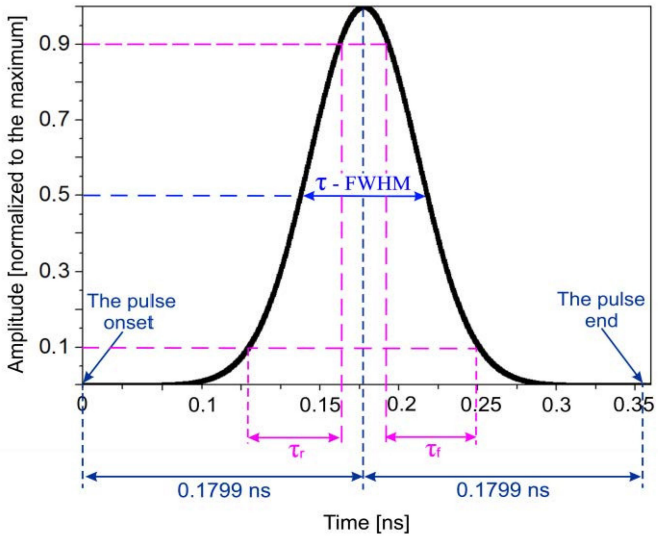

Figure 2. The time dependence of the electric field strength (or the magnetic field strength) of the normalized incident Gaussian EM plane wave pulse.

From a practical point of view, we introduce the incident pulse onset (or starting point) as a point preceding the pulse maximum by 0.1779 ns (Figure 2). Similarly, the end of the incident pulse is defined as a point 0.1779 ns after the pulse maximum. The electric and magnetic fields strengths are practically zero at both points. We set the time to t = 0

when the onset of the incident pulse reached the front wall plane of the enclosure; in other words, when the pulse maximum is 0.1779 ns in front of the enclosure front wall plane. This also means that at a time of 2 × 0.1779 ns = 0.3558 ns, the end of the incident pulse crosses the enclosure front wall plane and the direct impact of the incident pulse on the aperture ceases.

5. Results

The incident HPEM plane wave pulse affects the EM environment inside and around the enclosure with aperture by penetrating partly into the enclosure through the aperture and forming the electric charges and the electric currents in the enclosure walls which, in turn, create the associated electric and magnetic fields inside the enclosure, deforming the incident HPEM plane wave field outside the enclosure.

Therefore, the EM field formed inside the enclosure by the incident HPEM pulse is a superposition of that part of the transient incident EM pulse field (called, by us, the geometrical penetration field) which entered into the enclosure through the aperture in the way described by the geometrical (ray) optics, the electric field generated by the electric charges formed on the aperture edges and inner sides of the walls of the enclosure, and the magnetic field generated by the surface current formed on the aperture edges as well as on the inner walls of the enclosure.

Figure 3a,b illustrates the penetration of the electric field of the incident EM pulse into the enclosure at the early stage of the penetration at times t = 0.1375 ns and t = 0.1779 ns, respectively, in the plane y = 0 (the top view). At the very early stage of the incident pulse penetration into the enclosure at t = 0.1375 ns, it is possible to distinguish the geometrical penetration field (GPF) and the electric charge field (ECF). However, with time elapse (already at t = 0.1779 ns), the GPF and the ECF interfere strongly when moving deeper into the enclosure. According to this, our simulation yields the interference images of both fields (denoted GPF + ECF in Figure 3b) in the enclosure volume defined by the aperture boundary.

At the early penetration stage, the positive and negative electric charges gather at the aperture edges forming a dipol-like pair of the electric charges (Q_1+, Q_1-) (Figures 3 and 4a). Therefore, the range of impact of the ECF, produced by the electric dipol-like pair (Q_1+, Q_1-), is limited to the vicinity of the enclosure aperture (Figures 3 and 4a). When the incident pulse penetrates the enclosure deeper, the formation of the electric charges at the surface of the inner walls of the enclosure proceeds in the form of moving positive Q_i+ and negative Q_i- electric charge "islands" (i = 1, 2, 3, 4, etc.) at the enclosure inner walls (Figure 4b,c). Note that the charge values, shape, and positions of the "old" electric charges (Q_1+, Q_1-), and the newly formed charges (Q_i+, Q_i-) (i = 2, 3, 4, etc.), change as the incident pulse passes the enclosure. The corresponding positive Q_i+ and negative Q_i- charges form dipol-like pairs, which produce their own time-varying electric fields ECF_i (t) inside the enclosure. These fields interfere with each other, resulting in the time-varying electric field structures in the enclosure (structures E1, E2, and E4 in Figure 4a–c), respectively. The time-dependent structure E1 is the result of interference of GPF (t_1) and ECF_1 (t_1) at t_1 = 0.2179 ns. The structure E2 comes from the interference of GPF (t_2), ECF_1 (t_2), and ECF_2 (t_2). Similarly, the structure E4 is the interference of GPF (t_4), ECF_1 (t_4), ECF_2 (t_4), ECF_3 (t_4), and ECF_4 (t_4) at t_4 = 0.7000 ns. Note that t_1 is the time in which only the pair (Q_1+, Q_1-) exists, and t_2 is the time in which two pairs (Q_1+, Q_1-) and (Q_2+, Q_2-) exist. With elapsing time, new dipol-like pairs (Q_i+, Q_i-), i = 5, 6, 7, etc., and corresponding new ECF_i appear, causing the increased number of interferences. As a result, distinguishing the GPF and the ECF_i originating from the electric charge dipol-like pairs (Q_i+, Q_i-) becomes impossible at the later stage of the HPEM pulse penetration into the enclosure.

Similarly, the penetration of the magnetic field of the incident EM pulse into the enclosure can be described by following the development of the electric current on the surfaces of the enclosure inner walls.

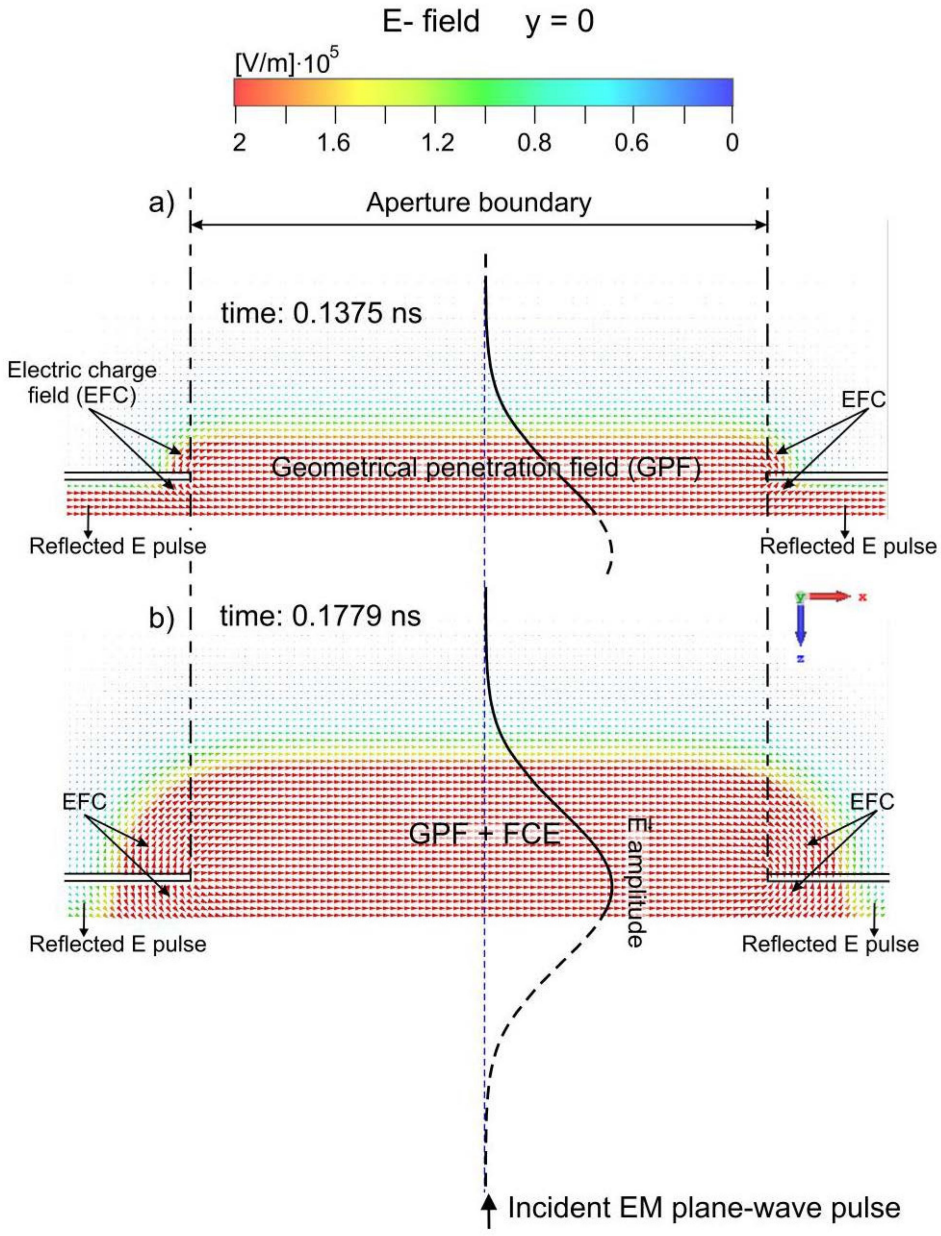

Figure 3. Illustration of the penetration and propagation of the electric field of the HPEM incident plane wave pulse in the enclosure at the early penetration stage for the area around the aperture: (**a**) t = 0.1375 ns, (**b**) t = 0.1779 ns in the plane y = 0 (the top view). GPF—the geometrical penetration field, ECF—the electric charge field. The color bar does not reflect the actual variation of the $\vec{E}$ amplitude for larger amplitudes (relay on the field profile $|\vec{E}|$).

The detailed analysis of the forming of the electric and magnetic fields inside the enclosure, taking into account the mechanisms of the formation of electric charges and currents at the surface of the enclosure walls the during interaction of the incident pulse with the aperture, is beyond the scope of this paper. Such analysis will be presented in another paper. The above short description of the interference-based mechanism of the electric field formation in the enclosure was intended only to explain why the images of the computer simulation of the electric field (and, by analogy, also the magnetic field) development in the later interaction stages presented below will be difficult to interpret.

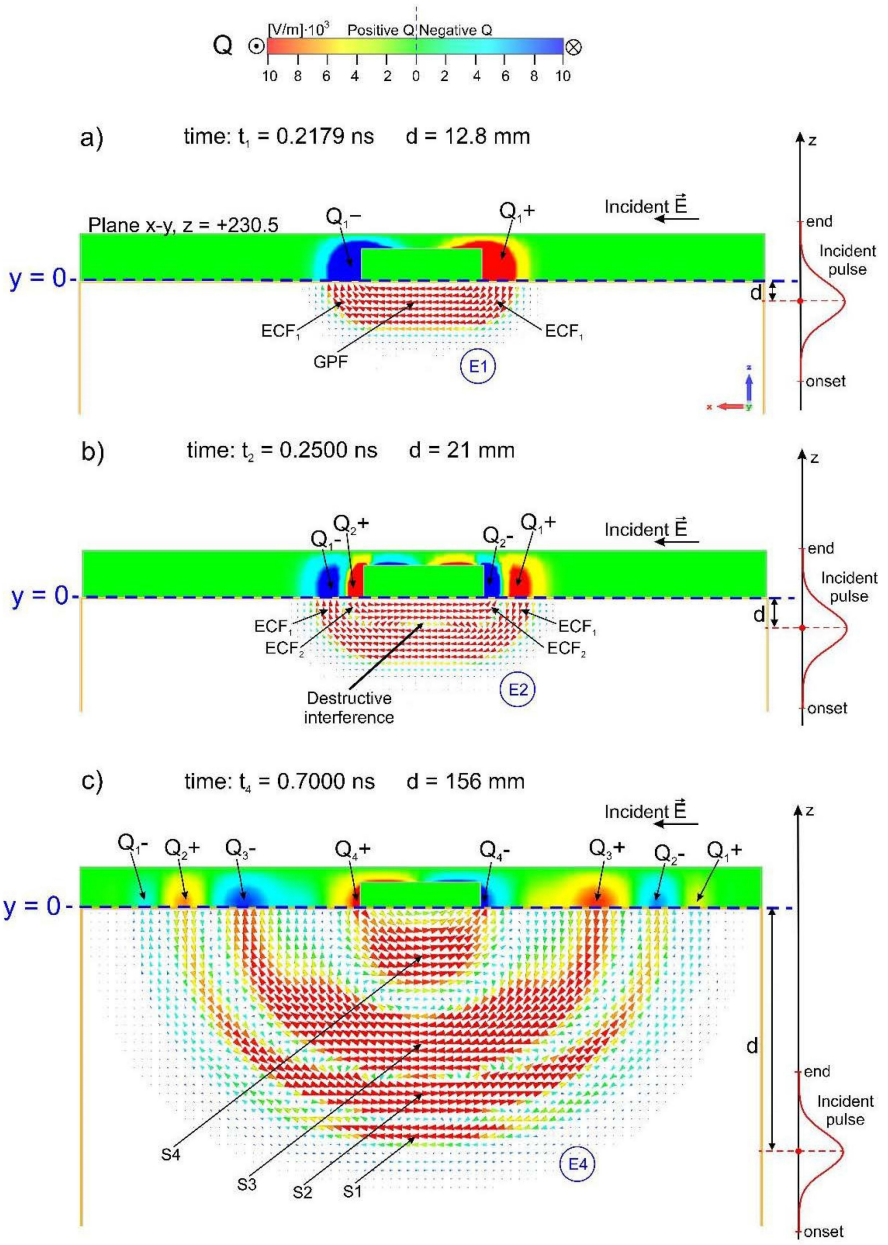

Figure 4. 2D development of the electric charge Q (positive Q_i+, negative Q_i-, i = 1, 2, 3, 4) on the inner side of the front wall plane of the enclosure (z = +230.5 mm) and electric field strength $\vec{E}$ in the x–z plane (y = 0) in the part of enclosure. E1, E2, E4—the electric field interference structures at times: 0.2179 ns, 0.2500 ns, and 0.7000 ns, respectively. The pair of electric charges (Q_i+, Q_i-) forms an electric dipol-like arrangement. d—the distance between the incident pulse maximum (marked in red dot) and the inner side of the front wall of the enclosure: (**a**) d = 12.8 mm (the half-maximum of the rear part of the incident pulse passes the front wall inner plane of the enclosure), (**b**) d = 21 mm (the one-tenth of the rear part of the incident pulse passes the front wall inner plane), (**c**) d = 156 mm (the incident pulse fully passed the enclosure front wall plane). The bold arrow in (**b**) shows the place in the E2 structure where the destructive interference occurred. S1, S2, S3, S4—the electric field interference substructures of the structure E4.

This paper focuses primarily on the results of computer simulation, i.e., the images of the electric and magnetic fields in the shielding enclosure with aperture when disturbed by the subnanosecond parallelly polarized HPEM plane wave. They are shown in Figure 5 (3D) and Figure 6 (2D).

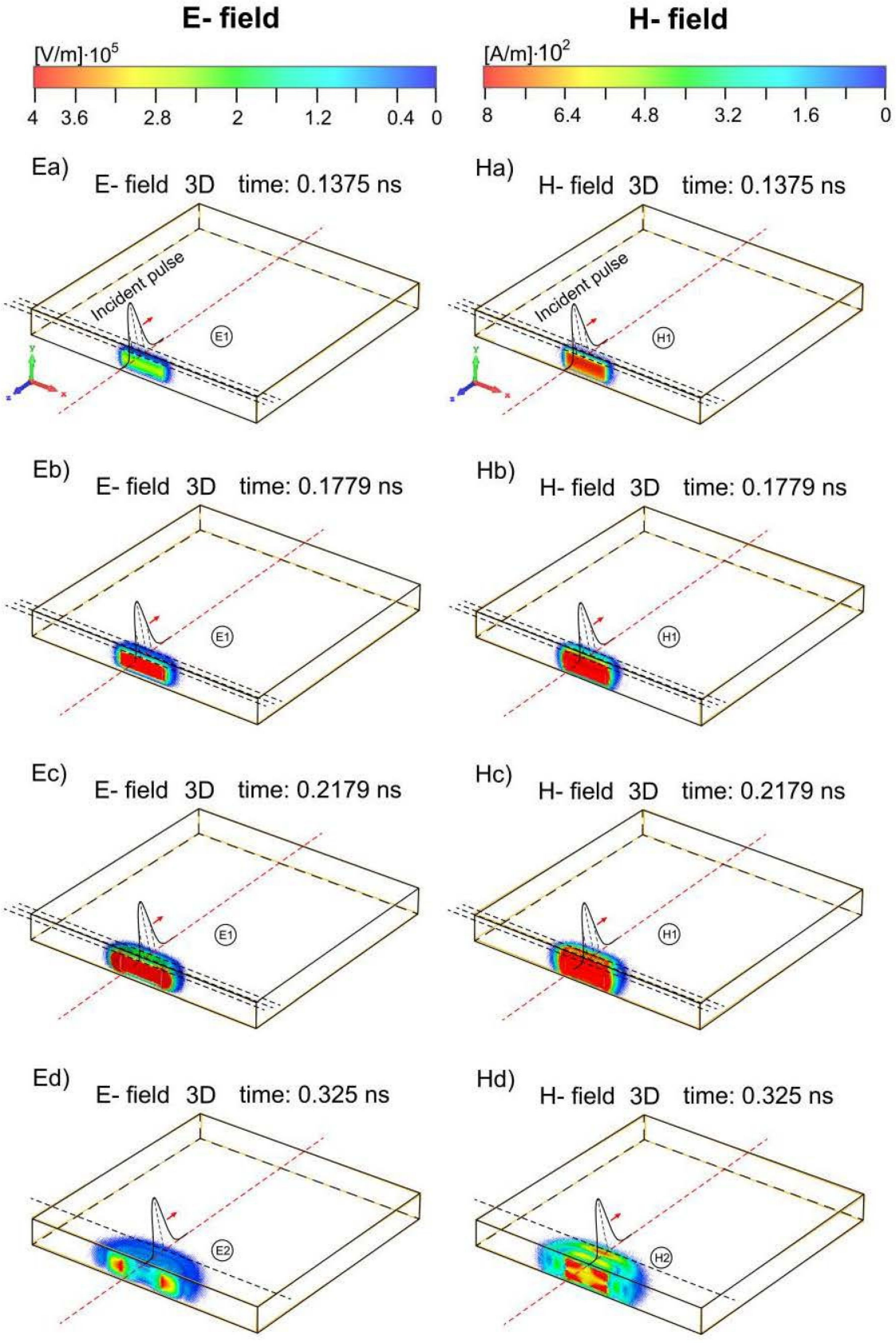

Figure 5. *Cont*.

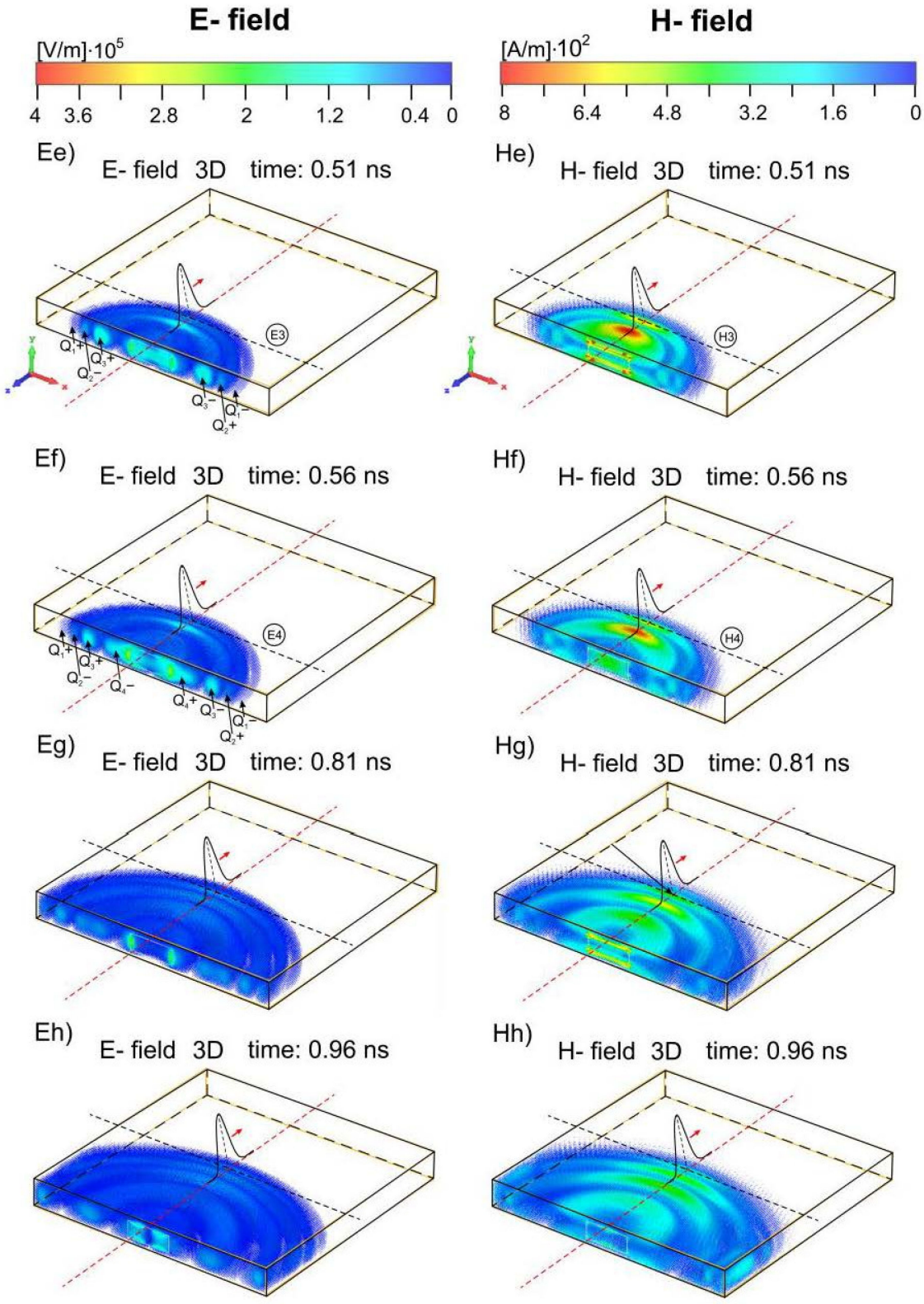

Figure 5. *Cont.*

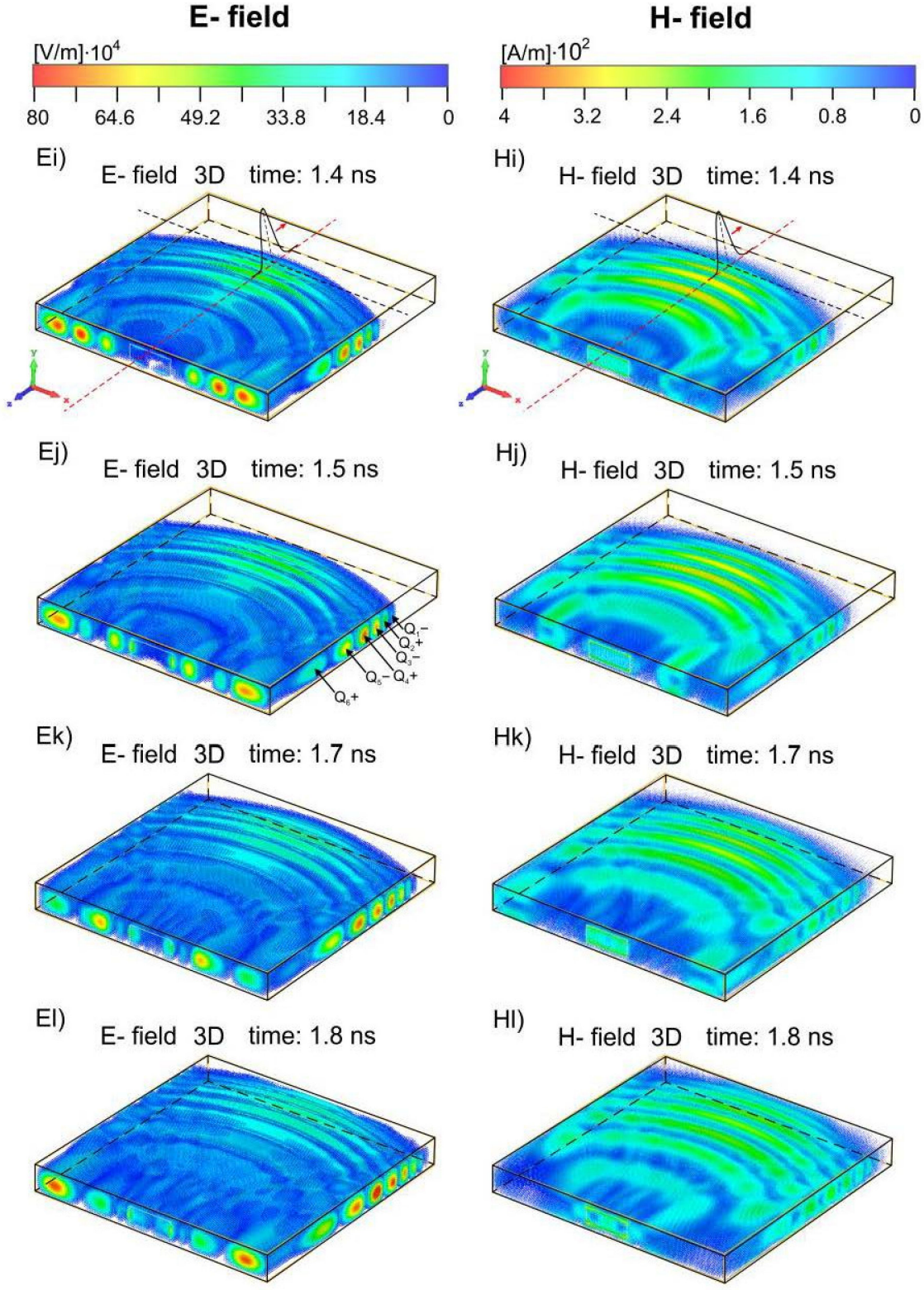

Figure 5. *Cont*.

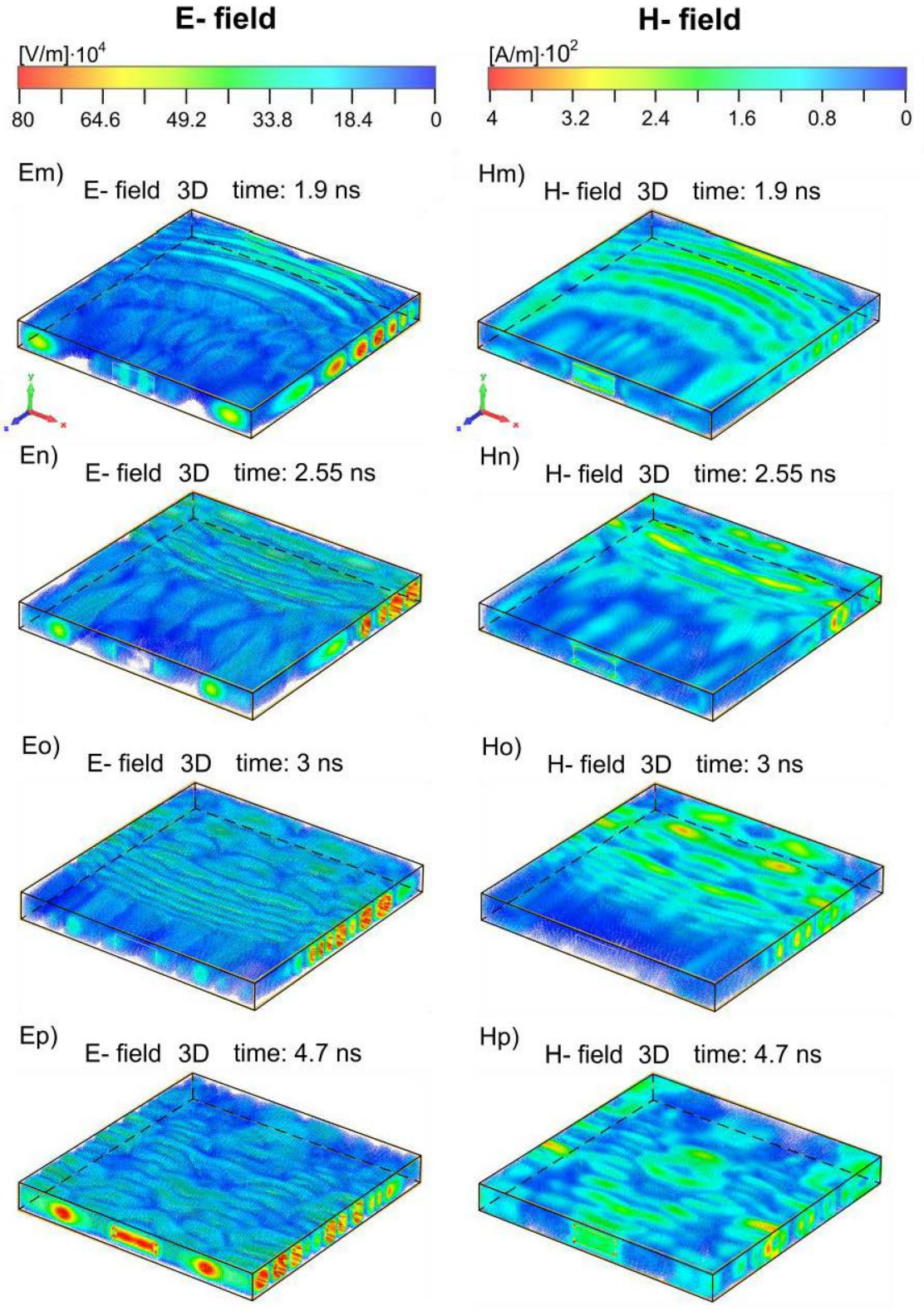

Figure 5. *Cont*.

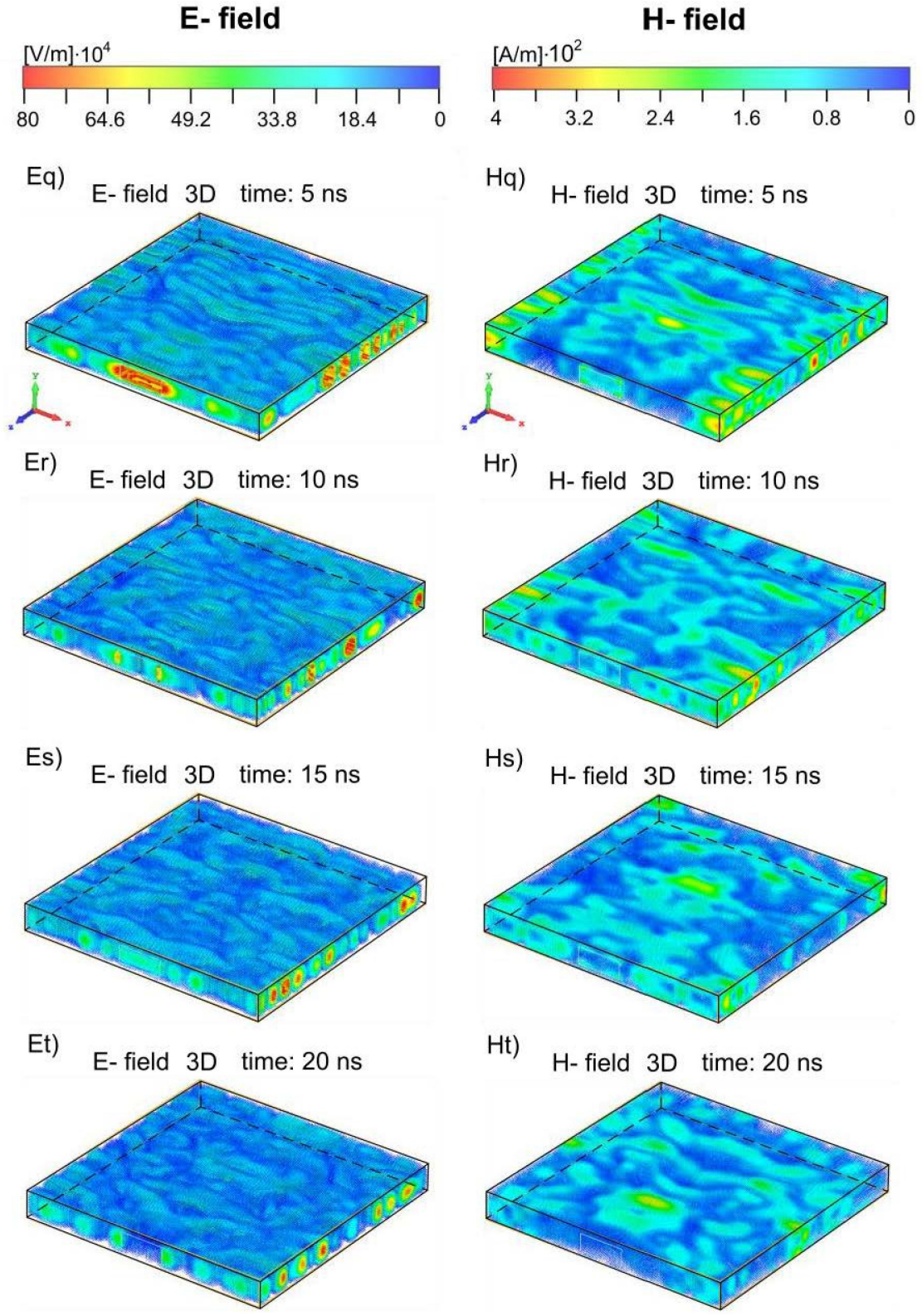

Figure 5. *Cont*.

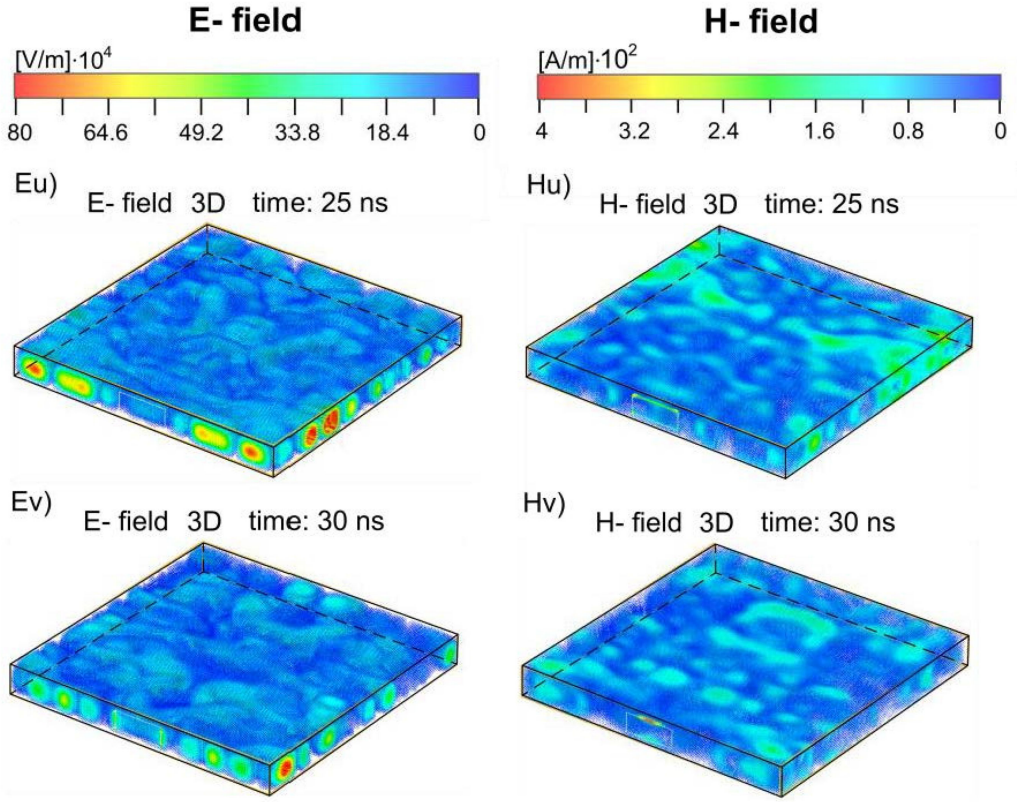

Figure 5. 3D development of the electric and magnetic fields in the enclosure. (**Ea**–**Ev**) the electric field amplitude; (**Ha**–**Hv**)—the magnetic field amplitude. The current position of the incident HPEM pulse is shown on the upper wall of the enclosure. E1, E2, E3, E4—the interference electric field structures. H1, H2, H3, H4—the interference magnetic field structures. The positions of the electric charges Q_i+ and Q_i- (i = 1, 2, 3, 4, 5, 6) at t = 0.51 ns, t = 0.56 ns, and t = 1.5 ns are shown in Figure 5Ee,Ef,Ej.

The simulation results presenting the formation, development, and decay of the EM in the enclosure were also recorded as video films. The video films show: (A) 3D electric field amplitude, (B) 3D magnetic field amplitude, (C) 2D electric field amplitude, and (D) 2D magnetic field amplitude (Supplementary Materials). Scan the QR code below to watch the films (Scheme 1). Much can be learned from these films about the behavior of the electric and magnetic fields in the apertured enclosure irradiated with the short-term EM pulse.

Scheme 1. QR code with link to video films.

Figure 5 visualizes the three-dimensional (3D) temporal and spatial development of the electric and magnetic fields in the apertured enclosure from the time t = 0 when the onset of the incident plane wave pulse reaches the front plane of the enclosure to the time t = 30 ns, i.e., when the incident HPEM pulse passed the enclosure and, being far from it, stopped affecting it. In Figure 5, the position of the incident EM plane wave pulse vs time is indicated on the upper wall of the enclosure. The temporal and spatial development of the electric field is shown in the left column, and that of the magnetic field in the right

column. Other details of the enclosure's electric and magnetic field evolution can be found in the two-dimensional (2D) Figure 6, and also in the vector maps for several cross-sections of the enclosure's interior (Figures 7–10).

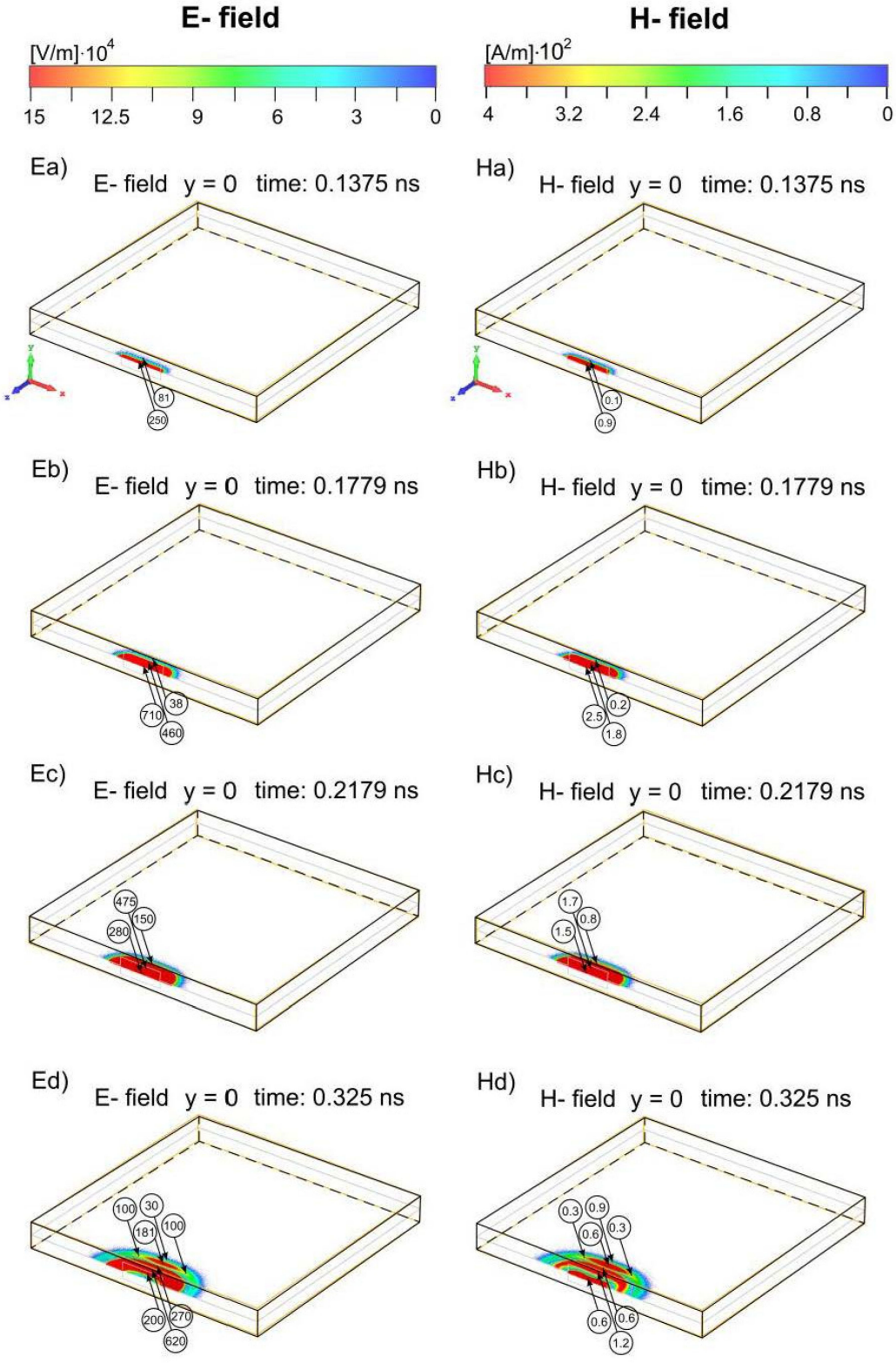

Figure 6. *Cont.*

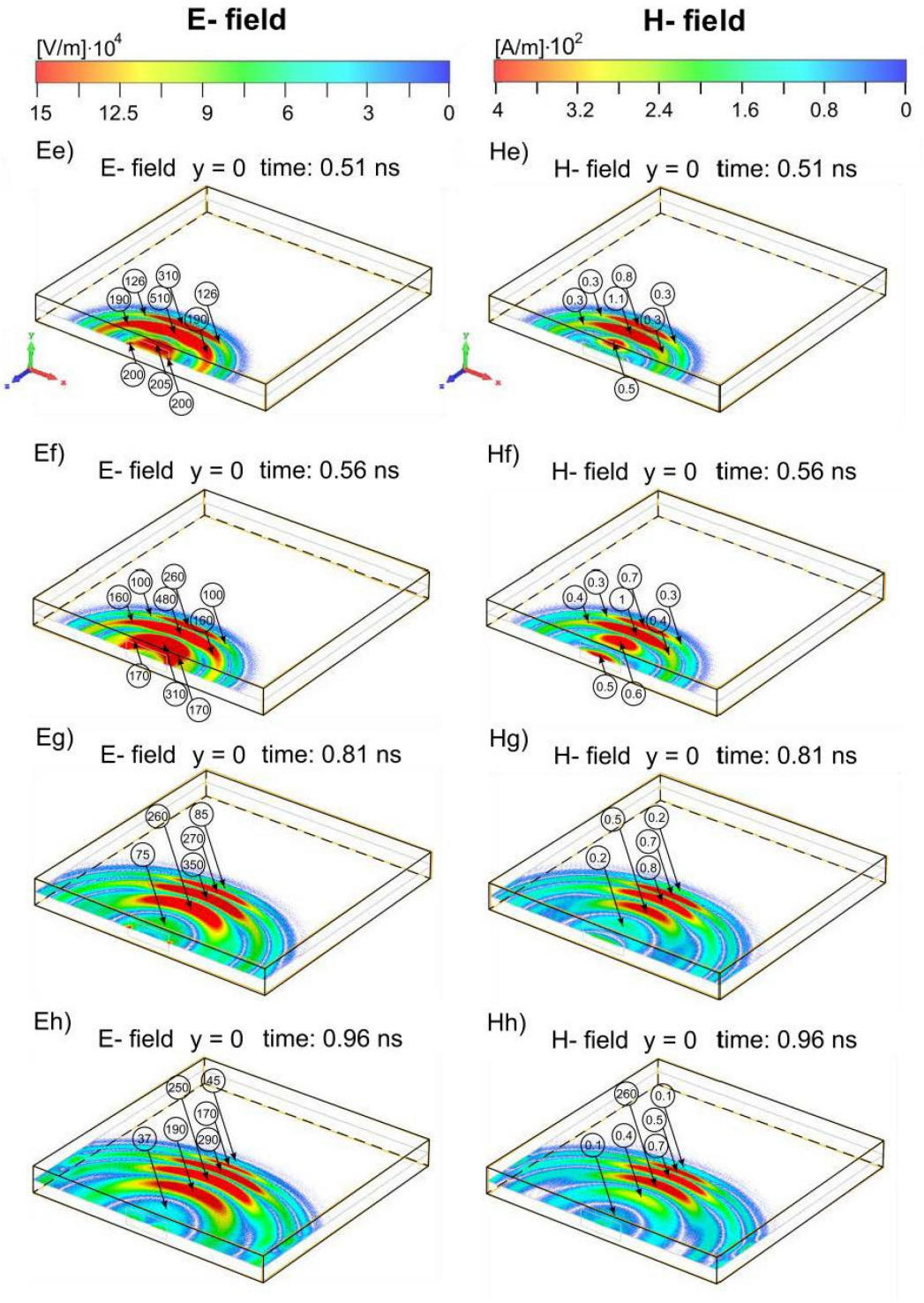

Figure 6. *Cont.*

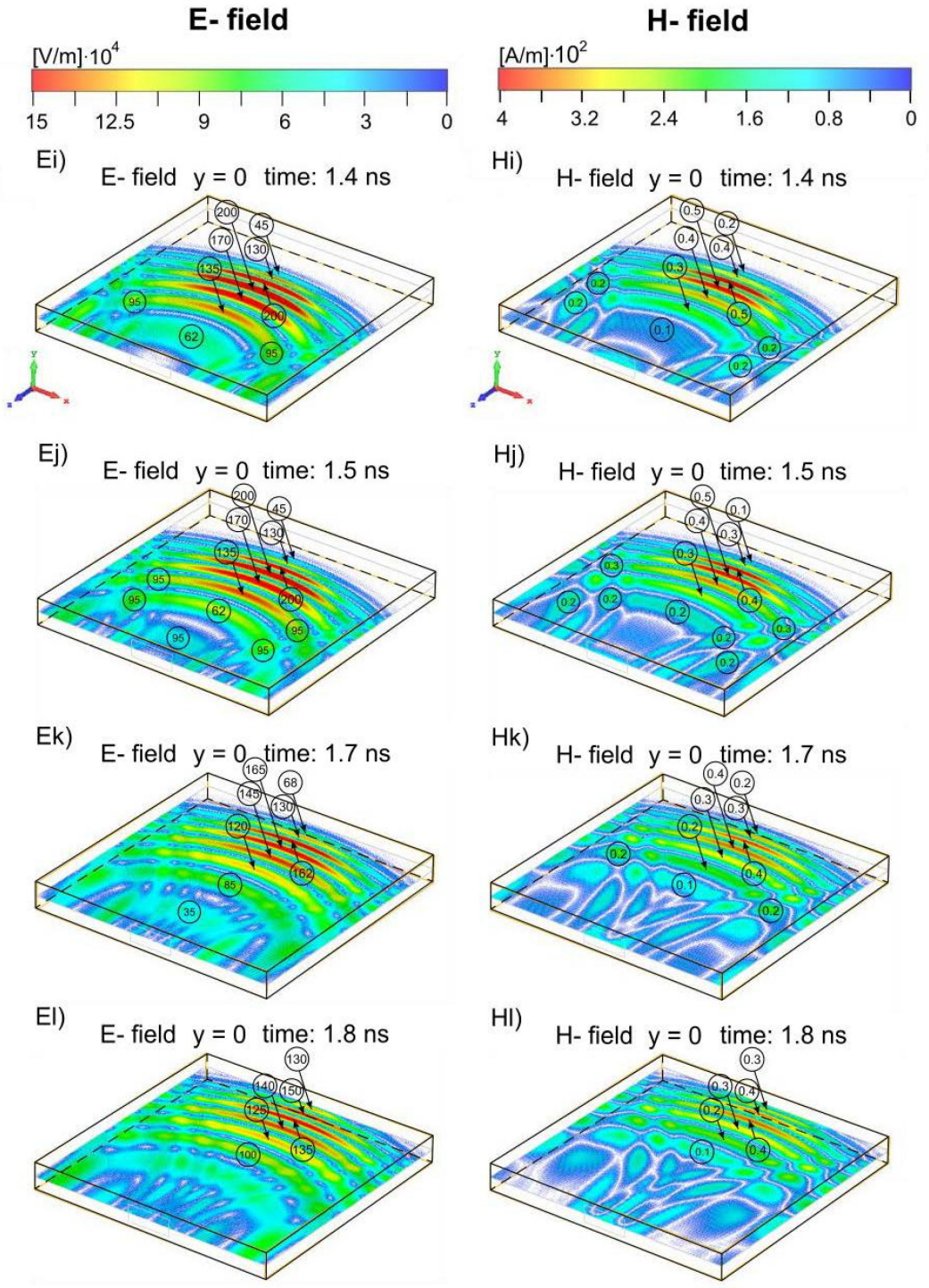

Figure 6. *Cont*.

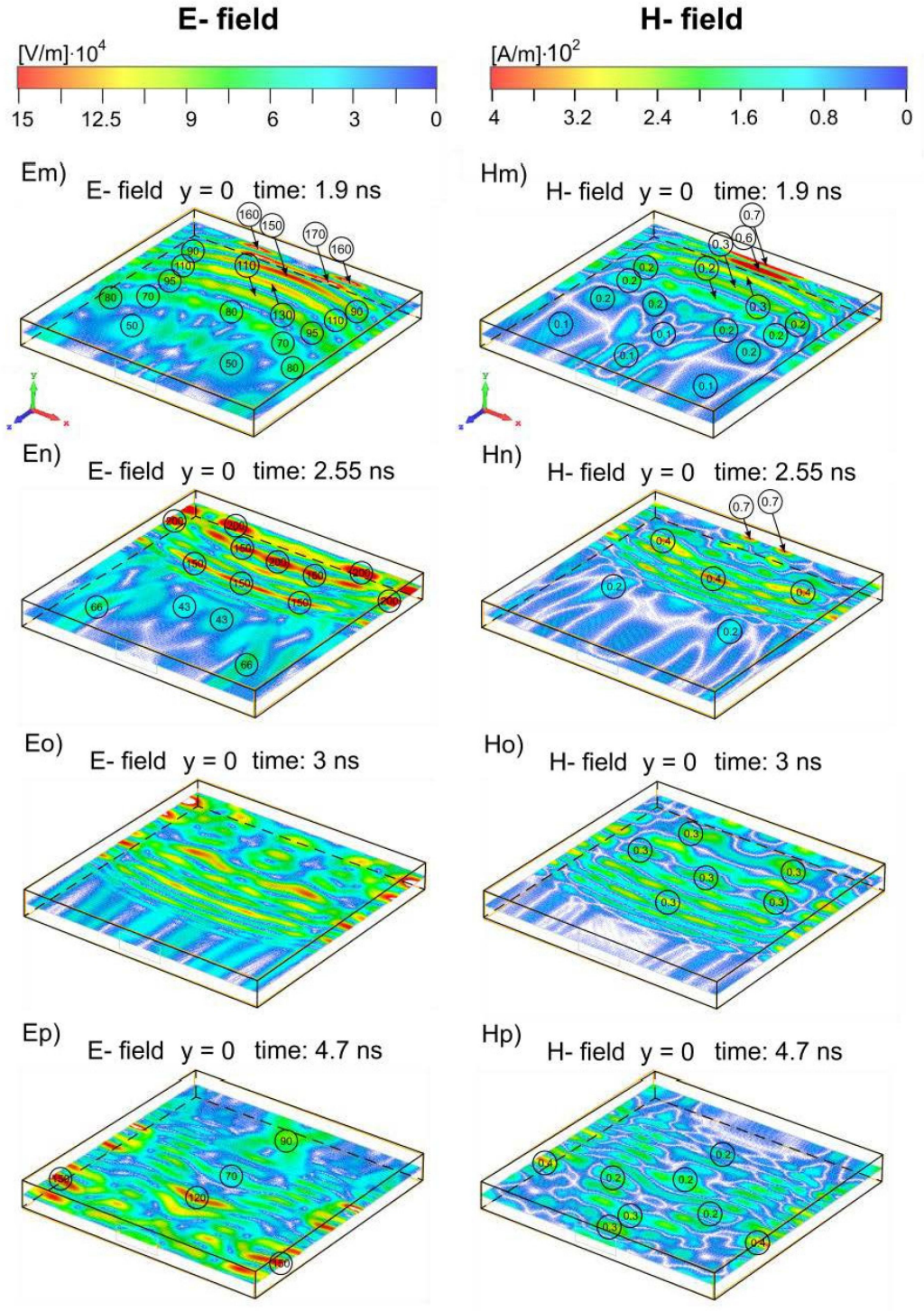

Figure 6. *Cont.*

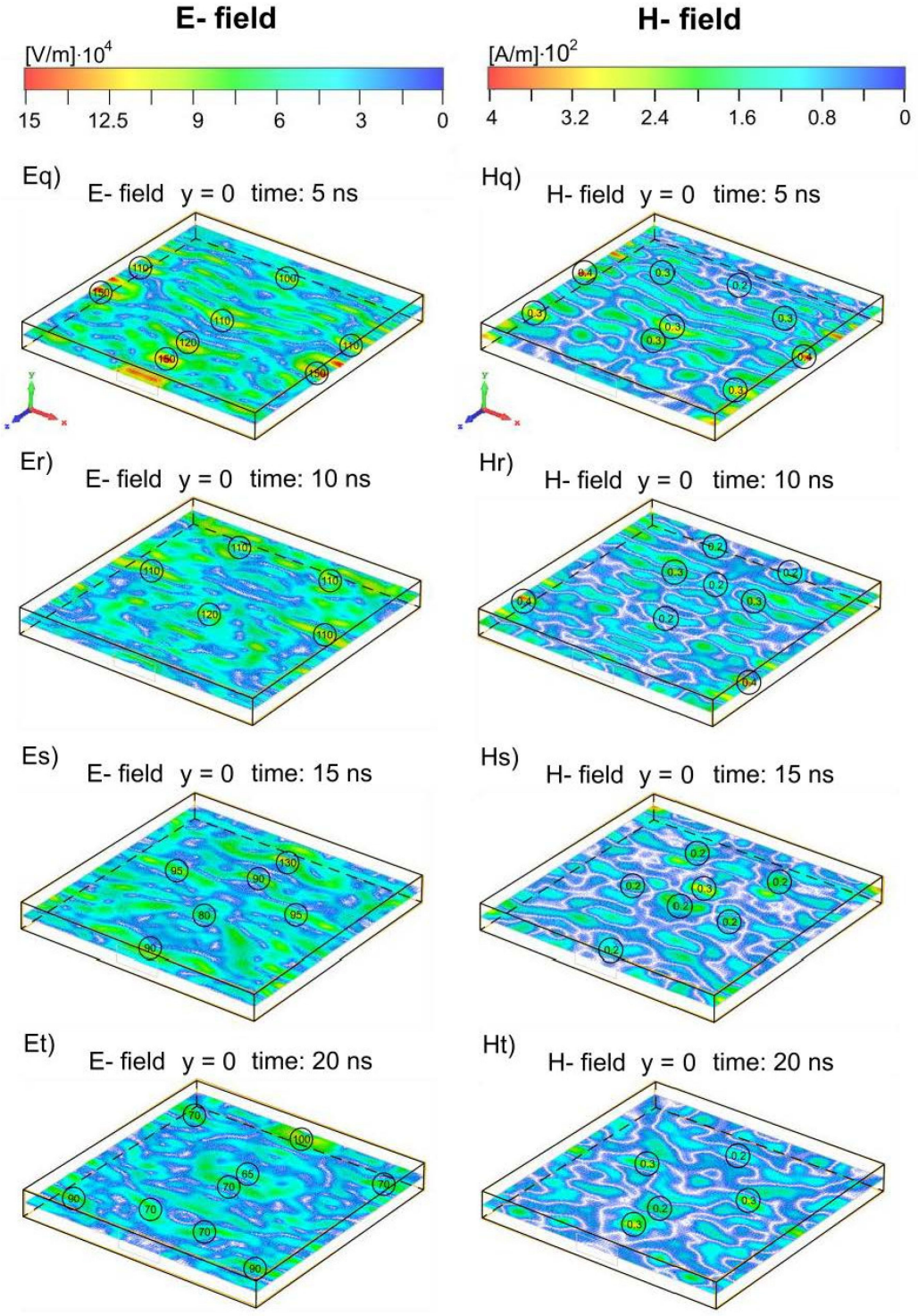

Figure 6. *Cont.*

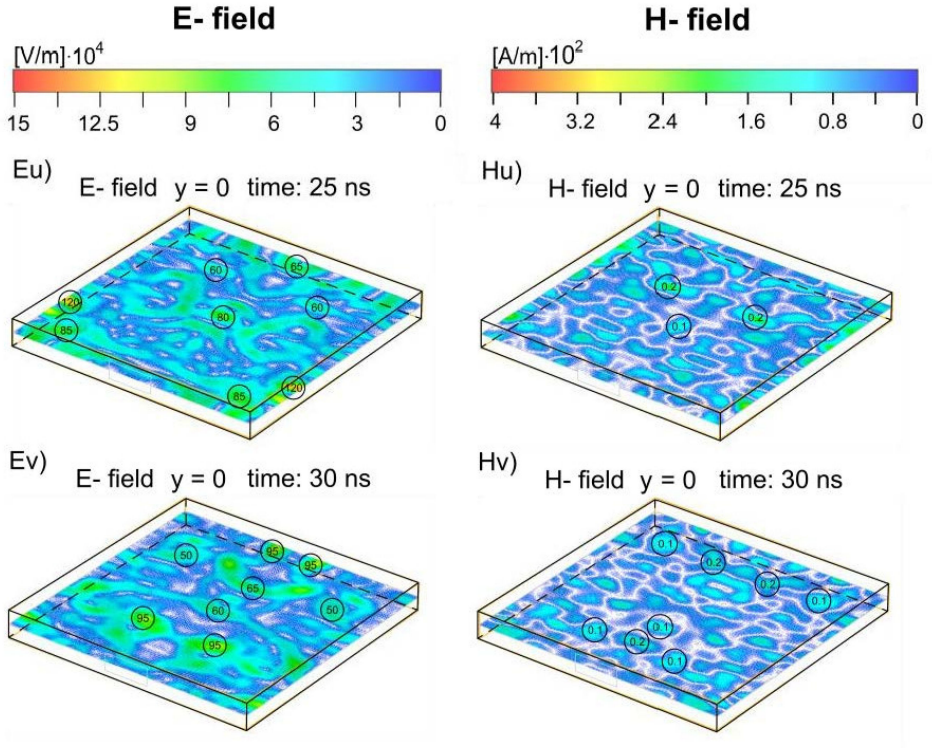

Figure 6. 2D development of the electric and magnetic fields in the enclosure. (**Ea**–**Ev**)—the electric field amplitude; (**Ha**–**Hv**)—the magnetic field amplitude. The amplitudes of the electric field (in 10^3 V/m) and the magnetic field (in 10^3 A/m) are given in circles.

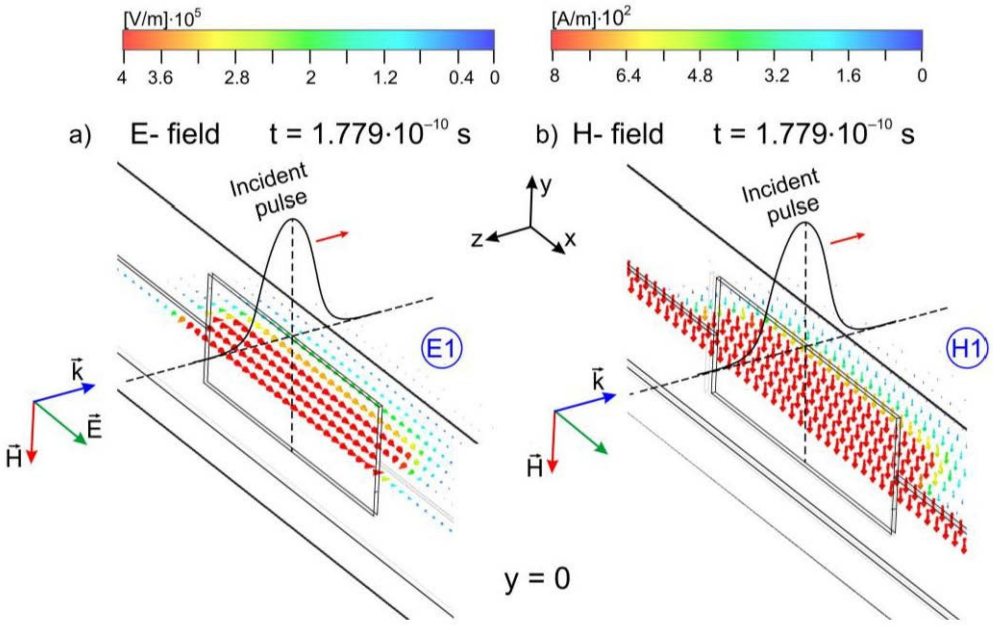

Figure 7. Associated electric E1 (**a**) and magnetic H1 (**b**) field structures in the plane xz (y = 0) at t = 0.1779 ns (i.e., when the incident pulse maximum passes the enclosure front wall plane). Vector $\vec{k}$ shows the propagation direction of the EM incident pulse. Retrieved from Figure 6Eb,Hb.

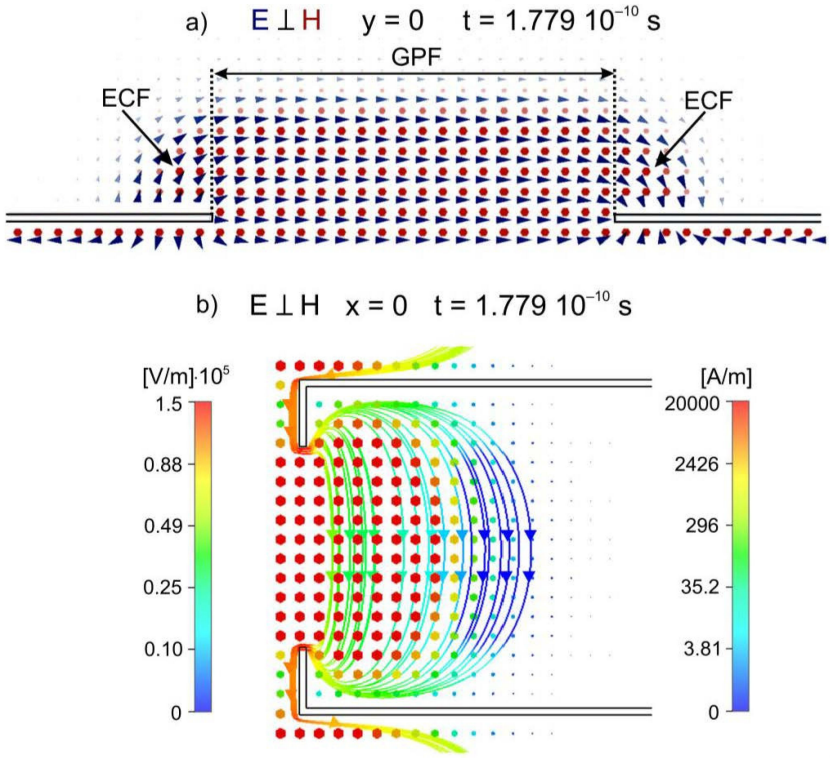

Figure 8. Associated electric (E1) and magnetic (H1) field structures at t = 0.1779 ns. (**a**) in the plane x-z (y = 0): the arrows show the electric field vectors, the dots show the magnetic field vectors which are perpendicular to plane y = 0 (facing away from the observer); color bar was not used to display the amplitudes, (**b**) in the plane y-z (x = 0): the dots show the electric field vectors (in logarithmic scale) which are perpendicular to plane y = 0 (directed to the observer); the isolines illustrate the fringing of magnetic field lines (in logarithmic scale) through the aperture into the enclosure. Retrieved from Figure 5Eb,Hb.

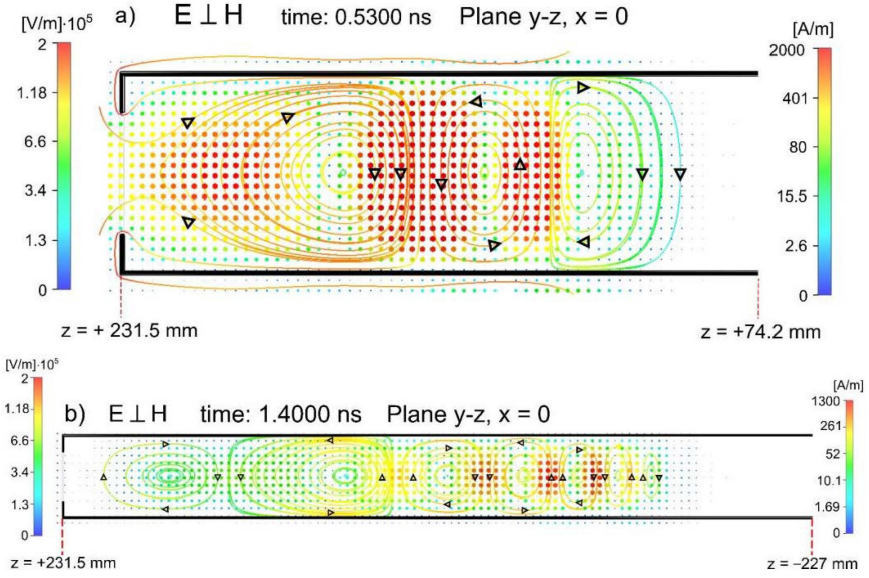

Figure 9. Associated electric and magnetic field structures in the plane y-z (x = 0): (**a**) at t = 0.530 ns (structures E4 and H4) and (**b**) at t = 1.400 ns. The dots show the electric field vectors, the isolines show the magnetic field lines (in logarithmic scale) in the enclosure. Retrieved from Figure 5Ei,Hi.

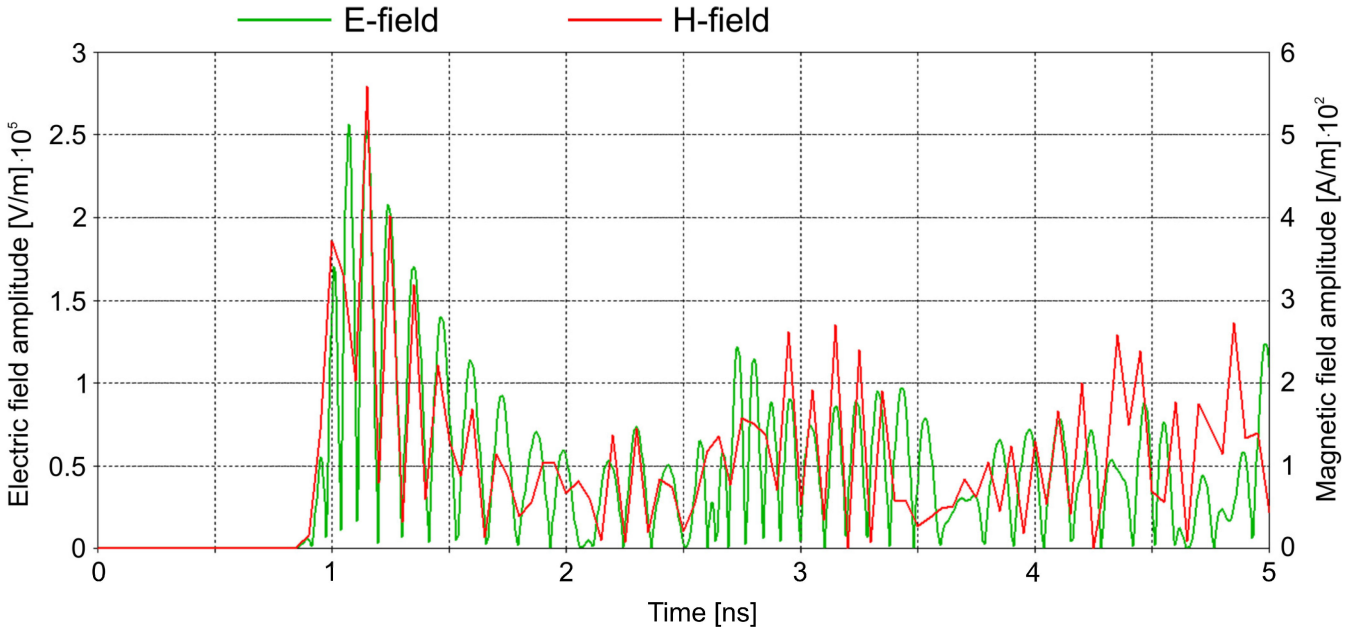

Figure 10. The time dependence of the amplitude of electric (marked in green line) and magnetic (marked in red line) fields strengths at point A (0,0,0) for parallel polarization of the incident plane-wave pulse of amplitudes 10^6 V/m and 2.68×10^3 A/m for the electric and magnetic fields, respectively. The peaks are called the electric and magnetic internal pulses.

It is seen from the images presented in Figures 5 and 6 that the incident HPEM pulse initiates an EM field in the aperture enclosure, which then propagates from the enclosure front wall towards its rear wall, and then back after the reflection from the rear wall. The successive reflections from the front and rear walls result in a time-varying EM field structure, which oscillates between the front and rear walls of the enclosure. During each reflection from the front wall, the EM field slightly fades out due to the presence of a kind of EM field loss channel through the aperture. In the later stages of the EM field development in the enclosure with aperture, the aperture determines the direction of the EM oscillation, making the enclosure with aperture behave like a waveguide rather than an EM resonator.

Figure 5Ea–Ec (also Figures 3, 4a and 6Ea–Ec) show the development of the interference structure E1 of the electric field at the early stage of the HPEM pulse penetration into the enclosure (time up to t = 0.2179 ns). As it was shown above, the structure E1 is the result of constructive interference of the GPF and the ECF_1 originating from the electric charge pair (Q_1+, Q_1−)—see Figure 4a.

Figures 4b, 5Ed and 6Ed show the interference structure E2 of the electric field in the time interval 0.2200 ns–0.3250 ns in which two pairs of the electric charge (Q_1+, Q_1−) and (Q_2+, Q_2−) exist. Thus, the E2 structure is the result of interference of GPF, ECF_1 (originating from the pair (Q_1+, Q_1−), and ECF_2 (originating from the pair (Q_2+, Q_2 −))—see Figure 4b. Note that the electric field ECF_2 produced by the pair (Q_2+, Q_2 –) is directly opposite to the fields GPF and ECF_1. This causes the interference of the GPF, ECF_1, and ECF_2 to be partly destructive. The bold arrow in Figure 4b shows the place in the E2 structure where the destructive interference occurred.

The structure E3 at t = 0.5100 ns, shown in Figures 5Ee and 6Ee, is the result of interference of GPF, ECF_1 (originating from the pair (Q_1+, Q_1−)), ECF_2 (originating from the pair (Q_2+, Q_2 −)), and ECF_3 (originating from the pair (Q_2+, Q_3 −)). The electric field ECF_3 produced by the pair (Q_3+, Q_3 –) is directed as that of the structure E1, and consequently opposite to ECF_2.

After the time t = 0.5100 ns, a new pair of the electric charge (Q_4+, Q_4−) appears on the inner surface of the enclosure front wall, which results in a new interference structure E4 at

t = 0.5600 ns (Figures 4c, 5Ef and 6Ef). Thus, the structure E4 results from the interference of GPF, ECF_1, ECF_2, ECF_3, and ECF_4.

In parallel to the development of the interference-originated electric field structures E1–E4, the interference-originated magnetic field structures H1–H4 are formed (Figures 5Ha–Hf and 6Ha–Hf). The structures E1–E4 and H1-H4 compose the associated electric and magnetic field structures in the enclosure (Figures 7 and 8).

Figure 7a,b shows separately the associated electric and magnetic vector fields in the y = 0 at the time t = 0.1779 ns. This is the time the incident pulse maximum passes the enclosure front wall plane. The electric vector field, shown in Figure 7a, consisting of GPF and ECF_1, is the first interference structure E1. The electric field vectors of the structure E1 lie in the plane y = 0 (i.e., in the same plane as those of the incident pulse). However, the electric field vectors, which can be assigned to GPF, point to the +x direction, while those corresponding to ECF are perpendicular or oblique to the +x direction. In the plane y = 0, the magnetic field vectors, forming the first interference structure H1, are directed in the −y direction, similarly to those in the incident pulse.

Figure 8a,b shows simultaneously the associated electric and magnetic fields of the structures E1 and H1, already presented separately in Figure 7a,b. In Figure 8a, the arrows show the electric field vectors, and the dots show the magnetic field vectors which are perpendicular to plane y = 0 (facing away from the observer). The associated electric and magnetic fields of the structures E1 and H1 in the plane x = 0 are simultaneously shown in Figure 8b. In Figure 8b, the isolines show the magnetic field lines, and the dots show the electric field which are perpendicular to the plane y = 0 (directed to the observer). Figure 8b illustrates how the tangential magnetic field lines fringe through the aperture into the enclosure. A similar manner of the magnetic field fringing was described for the case of an aperture in a conducting wall in [12].

Figure 9 shows simultaneously the developed electric and magnetic field structures in the plane x = 0 for the times t = 0.5300 ns (Figure 9a) and t = 1.4000 ns (Figure 9b). In both cases the incident pulse fully passed the enclosure aperture plane. At t = 0.5300 ns, when the electric charge pairs (Q_i+, Q_i−) are located only on the inner side of the enclosure front wall, the associated field structures E4 and H4 are present. At t = 1.4000 ns, when the incident pulse penetrated relatively deeply into the enclosure and the electric charge pairs (Q_i+, Q_i−) are also present on the inner side of the side walls of the enclosure, a more complex EM field structure develops. In both figures, Figure 9a,b, the closed loops of the magnetic field lines embracing the bundles of the electric field vectors are visible.

As already shown in Figure 9B, with elapsed time, when the incident pulse penetrated deeply into the enclosure, EM structures appear, which are more complex than the E1–E4 and H1–H4 structures presented so far. This is caused by new electric charge pairs (Q_i+, Q_i−), which also form on the inner side of the enclosure side walls. These new electric charge pairs (Q_i+, Q_i−) are clearly visible in Figure 5Ei (t = 1.400 ns)–5Ev (t = 30 ns). However, up to approximately t = 1.5 ns, i.e., before the reflection of the front of the electric and magnetic structures from the enclosure rear wall, we are still able to distinguish individual interference electric and magnetic structures (Figures 5Eg–Ej,Hg–Hj and 6Eg–Ej,Hg–Hj). After the reflection, due to the interference of the electric and magnetic structures moving toward and from the enclosure rear wall, we deal with a complex time-varying EM field rather than with the individual electric and magnetic structures. After the time t = 3 ns (Figures 5Eo,Ho and 6Eo,Ho), when the front of the EM field pattern first time reflected from the enclosure front wall, the EM field pattern has the form of time-varying interference areas of various shapes and sizes, which change with time. Additionally, the amplitudes of the electric and magnetic fields of these interference areas change with time. The whole EM field pattern, causing the interference areas, oscillates between the front and rear walls of the enclosure (Figures 5Ep–Ev,Hp–Hv and 6Ep–Ev,Hp–Hv). It is seen from these figures that the time-varying and size-limited areas that form the EM field pattern are placed symmetrically with respect to the z-axis. The highest amplitudes of the electric and magnetic fields occur in those interference areas which lie on the z-axis.

The results presented in Figures 5Ea–Ev,Ha–Hv and 6Ea–Ev,Ha–Hv show that the amplitudes of the electric and magnetic fields in the enclosure were lower than those of the incident EM plane wave pulse (10^6 V/m and 2.68 $\times$ 10^3 A/m for the electric and magnetic fields, respectively). For example, they substantially decreased within 30 ns after the interference of the EM plane wave pulse to about 6.5 $\times$ 10^4 V/m and 200 A/m, respectively (at the center of the enclosure at point A(0,0,0), Figures 5Hv and 6Ev).

The highest amplitudes of the electric and magnetic fields in the enclosure decrease with time. This is due to the tendency of the EM field pattern to fill the enclosure evenly, whereby the highest amplitudes of the electric and magnetic fields must decrease. Additionally, a part of the EM field energy leaves the enclosure through the aperture when the EM field pattern, oscillatory between the front and rear enclosure walls, reflects from the front wall.

It is easy to see from Figures 5 and 6 that the amplitudes of the electric and magnetic fields change with time at each point of the enclosure, when the time-varying EM field pattern appears between the front and rear walls of the enclosure. This is demonstrated in Figure 10, which shows the time dependence of the electric and magnetic fields at the central point A (0,0,0). It is seen from Figure 10, that the electric and magnetic fields at point A appear in the form of subnanosecond EM pulses, which we call the internal EM pulses. The internal EM pulse results from the corresponding EM area passing through point A (the first internal pulses of the electric field corresponding to the substructures S1–S4 belonging to the structure E4—Figure 4). The amplitudes of the internal pulses are lower than those of the incident EM pulse. The amplitudes of the first internal pulses are about 2 $\times$ 10^5 V/m and 400 A/m for the electric and magnetic fields, respectively. They decrease non-monotonic with time to about 0.7 $\times$ 10^5 V/m and 200 A/m at t = 5 ns.

Similar behavior of the EM field as shown in Figure 10 can be found for the other points inside the enclosure.

The above shows that using the enclosure with aperture as an EM shielding changes the character of the disturbance caused by the subnanosecond EM pulse. In the case of a direct action of the subnanosecond EM pulse on an unsecured (in the absence of the enclosure) point, the impact of this pulse is a one-time act, i.e., the high EM field affects this point only once in the subnanosecond period. However, after applying the enclosure with aperture to shield the point, the time of influence on this point by the EM field developed in the enclosure in the form of internal EM pulses significantly increases. In the enclosure with aperture, the series of subnanosecond EM internal pulses persist for at least 30 ns. This means that point A in the enclosure is influenced repeatedly over 30 ns by about 900 subnanosecond EM internal pulses. In general, the amplitudes of the EM internal pulses are lower than that of the EM incident pulse, in particular for a time longer than 10 ns (by a factor greater than 10). However, a few first EM internal pulses whose amplitude is only 6 times lower than that of the incident pulse (Figure 10) may pose a severe EM hazard. Therefore, the generation of the subnanosecond EM internal pulses in the enclosure with amplitudes differing only by 6-times from the incident pulse amplitude is a serious threat. It is known that the extent of damage caused to advanced electronic devices depends not only on the power (or energy) of EM radiation pulses but also on their persistence (number of repetitions of the interference). As shown in [13], some electronic devices are more susceptible to pulses if applied with a higher repetition rate despite their lower electric or magnetic field strength amplitudes. In this case, the effectiveness of EM shielding by the enclosure with aperture can be questioned.

6. Conclusions

This paper shows the results of the numerical simulations of the development of the EM field in the shielding enclosure with aperture after the interference of the subnanosecond high-power EM plane wave pulse, which had the parallel polarization.

In the case described in this paper, the numerical simulation of the coupling and development of an EM field inside the enclosure allows visual tracking of the successive stages of the electric and magnetic field development within 30 ns.

We presented 2D and 3D images along with vector maps showing the development and form of the electric and magnetic fields inside the enclosure, and the distribution of the electric charges on the inner walls of the enclosure over 30 ns after the interference of the subnanosecond high-power EM plane wave pulse. Other studies on the interaction of transient high-power EM pulses with apertured enclosures concerned mostly cases with pulses of duration over 150 ns. In our case, the full duration of the incident EM pulse was $\tau = 0.3558$ ns. This means that the EM pulse duration is much shorter than the time taken for the pulse to pass the enclosure. Such a long observation time relative to the duration of the incident EM pulse (more than about 300 times longer) enables us to track in detail the changes in the EM field inside the apertured enclosure under study.

The numerical simulation of the development of the EM field inside the enclosure resulted in 2D and 3D images that enabled us to observe detailed tracking of the HPEM pulse penetration into the enclosure. The EM field formed in the enclosure with aperture has the form of the electric and magnetic field interference structures. At the early penetration stages, the positive and negative electric charges gathered at the aperture edges, formed the electric charge pairs (Q_i+, Q_i-) (i = 1, 2, 3, 4, etc.) which produced time-varying electric interference fields ECF_i inside the enclosure. These fields interfered with the geometrical penetration field, resulting in the time-varying electric E1–E4 and magnetic H1–H4 field structures. These electric and magnetic structures consisted of substructures, which appear in the form of subnanosecond EM pulses. We call these subnanosecond EM pulses internal EM pulses. The internal EM pulse results from the corresponding EM area passing through point A (the first internal pulses of the electric field corresponding to the substructures S1-S4 belonging to the structure E4. When the incident pulse penetrates the enclosure deeper, the formation of the electric charges at the surface of the inner walls of the enclosure proceeds in the form of moving positive Q_i+ and negative Q_i- electric charge "islands" at the enclosure inner walls. The results of the oscillation of the time-varying, EM field pattern between the front and rear walls of the enclosure, are EM field structures in the enclosure. At the later penetration stages, the EM field pattern has the form of a time-varying interference pattern. These varying interference patterns are complex, and it is difficult to understand and recognize the individual electric and magnetic structures inside the enclosure with aperture.

The EM field induced in the enclosure is long-lasting compared to the interference pulse duration. The amplitudes of the first internal pulses at the central point A (0,0,0) decrease to about 2×10^5 V/m and 400 A/m for the electric and magnetic fields, respectively. At the later penetration stages, they decrease non-monotonic with time to about 0.7×10^5 V/m and 200 A/m at $t = 5$ ns. Those amplitudes can still be a severe hazard to electronic devices placed in the enclosure with aperture.

The analysis of the shielding effectiveness of the apertured enclosure under ultrashort transient interference conditions provides an opportunity to more deeply understand the coupling and development mechanisms of the EM field induced inside a small apertured enclosure.

The studies of apertured enclosure shielding effectiveness against subnanosecond high-power pulses are lacking compared to studies with pulses of duration over hundreds of nanoseconds or longer. The case we have described on the effects of ultrashort high-power EM pulses involving parallel polarization provides a contribution to better understand the phenomena and mechanisms occurring inside apertured shielding enclosures after penetration of a disturbance pulse.

The 2D and 3D images obtained in this paper for the parallel polarization of the incident EM pulse differ from those of the perpendicularly polarized incident EM pulse shown in our previous work [4]. Due to the article's brevity, these differences will be the subject of another article.

Supplementary Materials: The following are available online at https://www.youtube.com/playlist?list=PLF9elidkw1nfcuyGiU8sprwOkOTJqKsUw (accessed on 1 November 2022) Videos: (A) 3D electric field magnitude, (B) 3D Magnetic field magnitude, (C) 2D electric field magnitude, and (D) 2D magnetic field magnitude.

Author Contributions: Conceptualization, M.B. and J.M.; methodology, M.B. and J.M.; investigation, M.B., J.M. and K.B.; writing—original draft preparation, M.B. and J.M.; writing—review and editing M.B., J.M. and K.B.; visualization, M.B. and J.M.; supervision, M.B. and J.M. All authors have read and agreed to the published version of the manuscript.

Funding: The project was financed within the program of the Ministry of Science and Higher Education called "Regionalna Inicjatywa Doskonałości" in the years 2019–2022; the project number was 006/RID/2018/19 and the sum of financing was PLN 11,870,000.

Institutional Review Board Statement: Not applicable.

Informed Consent Statement: Not applicable.

Data Availability Statement: Data sharing not applicable.

Conflicts of Interest: The authors declare no conflict of interest.

References

1. Sabath, F. System oriented view on high-power electromagnetic (HPEM) effects and intentional electromagnetic interference (IEMI). In Proceedings of the XXIX URSI General Assembly, Chicago, IL, USA, 7–16 August 2008.
2. Giri, D.V.; Tesche, F.M. Classification of Intentional Electromagnetic Environments (IEME). *IEEE Trans. Electromagn. Compat.* **2004**, *46*, 322–328. [CrossRef]
3. *IEC 61000-2-13*; Electromagnetic Compatibility (EMC)—Part 2–13: Environment—High-Power Electromagnetic (HPEM) Environments—Radiated and Conducted. 1st ed. International Electrotechnical Commission: Geneva, Switzerland, 2005.
4. Budnarowska, M.; Mizeraczyk, J. Temporal and Spatial Development of the EM Field in a Shielding Enclosure with Aperture after Transient Interference Caused by a Subnanosecond High-Energy EM Plane Wave Pulse. *Energies* **2021**, *14*, 3884. [CrossRef]
5. Sabath, F. *Threads of Electromagnetic Terrorism, EUROEM 2012*; ONERA: Toulouse, France, 2012; p. 17.
6. Shubitidze, P.; Jobava, R.; Karkashadze, D.; Beria, R.; Pommerenke, D.; Frei, S. Numerical study of the coupling of transient fields of ESD into a cavity. In Proceedings of the 4th International Seminar/Workshop on Direct and Inverse Problems of Electromagnetic and Acoustic Wave Theory (IEEE Cat. No.99TH8402), Lviv, Ukraine, 21–24 May 1998; pp. 108–110.
7. Celozzi, S.; Araneo, R. Alternative definitions for the time-domain shielding effectiveness of enclosures. *IEEE Trans. Electromagn. Compat.* **2014**, *56*, 482–485. [CrossRef]
8. Azizi, H.; Belkacem, F.T.; Moussaoui, D.; Moulai, H.; Bendaoud, A.; Bensetti, M. Electromagnetic interference from shielding effectiveness of a rectangular enclosure with apertures–circuital approach, FDTD and FIT modeling. *J. Electromagn. Waves Appl.* **2014**, *28*, 494–514. [CrossRef]
9. Ziolkowski, R.W. FDTD modelling of Gaussian beam interactions with metallic and dielectric nonostructures. In Proceedings of the URSI Electromagnetic Theory Symposium, Pisa, Italy, 23–27 May 2004; pp. 27–32.
10. Robinson, M.P.; Turner, J.D.; Thomas, D.W.P.; Dawson, J.F.; Ganley, M.D.; Marvin, A.C.; Porter, S.J.; Benson, T.M.; Christopoulos, C. Shielding effectiveness of a rectangular enclosure with a rectangular aperture. *Electron. Lett.* **1996**, *32*, 1559–1560. [CrossRef]
11. Available online: www.cst.com (accessed on 1 November 2022).
12. Colling, R.E. *Foundations for Microwave Engineering*, 2nd ed.; Mcgraw Hill Higher Education: New York, NY, USA, 1992; p. 284.
13. Korte, S.; Garbe, H. Breakdown Behaviour of electronics at variable pulse repetition rates. *Adv. Radio Sci.* **2006**, *4*, 7–10. [CrossRef]